International Journal of Innovative Research and Scientific Studies, 8(6) 2025, pages: 1317-1332

IJIRSS
International Journal of Innovative Research & Scientific Studies

ISSN: 2617-6548

URL: www.ijirss.com

Scandium enrichment in the Mandiodo nickel laterite, North Konawe, southeast Sulawesi

Yoseph H Paskarino[1,2*], Ghaly Yana Putra[1], Sutarto[1], Joko Soesilo[1], Bronto Sutopo[2]

[1]*Teknik Geologi UPN "Veteran" Yogyakarta, Indonesia.*
[2]*PT ANTAM Tbk, Indonesia.*

Corresponding author: Yoseph H Paskarino (*Email: 311212002@student.upnyk.ac.id*)

Abstract

Scandium is one of the heavy rare earth elements essential in various metal and energy industries. Indonesia has the potential to contain more than 4,000 tonnes of scandium, primarily in nickel laterites. The Mandiodo region is characterized by ultramafic rocks, which are part of the East Sulawesi Ophiolite complex, known for producing nickel laterite deposits. This study aims to identify indications of scandium enrichment within Mandiodo's nickel laterite deposits. Identification was conducted using pulp samples from three drill holes. Multiple analytical methods were employed to determine the geochemical properties of the laterite, weathering intensity, scandium content, mineralogical composition, mineral characteristics, rock genesis, the presence of metallic minerals in the bedrock, and scandium-bearing minerals within the bedrock. Results indicate that scandium is enriched in the limonite zone, at depths of 1-15 meters, residually with grades reaching up to 104 ppm. The scandium content shows a positive correlation with Al2O3, Fe2O3, and Cr2O3. The minerals present in the scandium-enriched zone are predominantly goethite, hematite, and talc. The content of goethite and the degree of weathering exhibit patterns similar to scandium distribution. Scandium is mainly hosted in the minerals augite and diopside, which crystallize through exsolution processes driven by temperature variations and aluminum content in the magma.

Keywords: Enrichment, Exsolution, Nickel, Laterite, Rare earth element, Scandium.

DOI: 10.53894/ijirss.v8i6.9913
Funding: This study received no specific financial support.
History: Received: 21 July 2025 / **Revised:** 25 August 2025 / **Accepted:** 27 August 2025 / **Published:** 18 September 2025

Competing Interests: The authors declare that they have no competing interests.
Authors' Contributions: All authors contributed equally to the conception and design of the study. All authors have read and agreed to the published version of the manuscript.
Transparency: The authors confirm that the manuscript is an honest, accurate, and transparent account of the study; that no vital features of the study have been omitted; and that any discrepancies from the study as planned have been explained. This study followed all ethical practices during writing.
Publisher: Innovative Research Publishing

1. Introduction

North Konawe Area has the potential for a high average grade of scandium, which is 91.21 ppm at Tapunopaka and 82 ppm at Bahubulu Island. These areas are enriched in the nickel laterite limonite zone with a thickness of 25-50 meters [1]. Scandium can be enriched in lateritic ultramafic rocks because these rocks can contain 6-80 ppm of scandium bound in

olivine or pyroxene through metal substitution [2]. Based on Teitler et al. [3], the scandium grade in the rocks of origin are successively dunite < peridotite < gabbro/basalt < amphibolite/pyroxenite.

Some previous studies include Simandjuntak and Barber [4]; Monnier et al. [5]; Parkinson [6] and Harris [7]; Kadarusman et al. [8] stated that the subduction or collision of the Australian Plate, Pacific Plate, and Eurasian Plate gave rise to a series of islands, folds, plate margin basins, continental fragments or microplates, and ophiolite complexes in Eastern Indonesia (Figure 2). Sulawesi Island, which has a shape similar to the letter "K," is believed to be a result of convergent activity between the East Java-West Sulawesi microplate in the West Central to South (as part of the Eurasian Plate), Buton-Tukang Besi in the Southeast, Banggai-Sula in the East Central (as part of the Australian Plate), and Caroline (as part of the Philippine Plate) in the North, which produced horizontal and strike-slip faults that raised the ofiolite complex to the surface, especially at the East arm and Southeast arm [9] where North Konawe District and Mandiodo Area located.

The geomorphology of the Mandiodo Block is classified into three main units: steep hills, flat plains, and alluvial plains. The steep hill morphology dominates the central and western parts of the block, with elevations reaching up to 500 meters above sea level (m asl) and characterized by rugged topographic texture. The alluvial plain is in the northern part of the block, with elevations below 50 m asl, and is typified by the presence of unconsolidated fluvial deposits. The intermediate plain morphology lies at elevations between 10–50 m asl and is slightly higher than the adjacent alluvial plains.

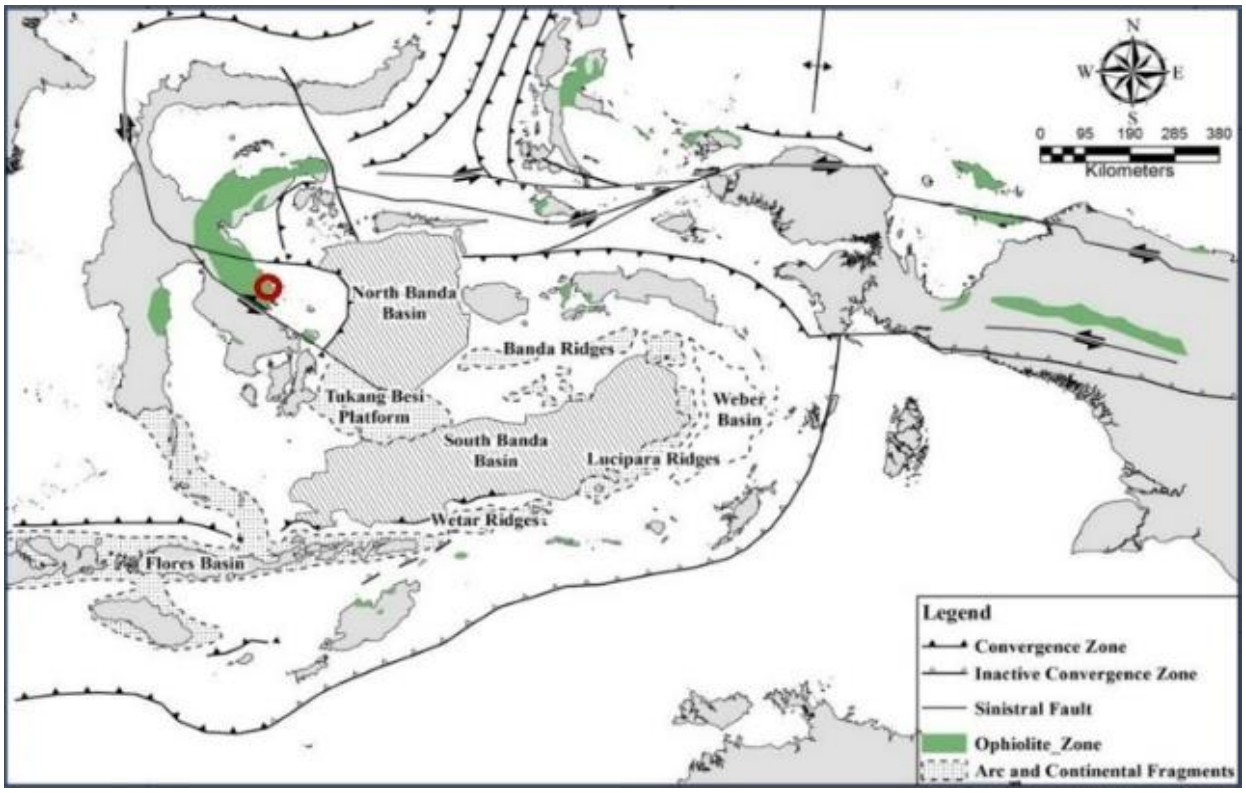

Figure 1.
Eastern Indonesia tectonic maps (modified from Harris [7]).

The lithologies observed in the Mandiodo Block include harzburgite and dunite units [10]. Harzburgite appears dark grey to greenish grey, exhibiting a holocrystalline texture with fine to medium phaneritic grain size, euhedral to subhedral crystal habit, and a panidiomorphic to hypidiomorphic equigranular texture. The rock is massive in structure and primarily composed of olivine (75%), pyroxene (15%), serpentine (3%), and iron oxides (7%), with silica and serpentine commonly filling fractures. Microscopically, harzburgite contains fine to coarse grains, consisting of olivine (60%), orthopyroxene (10%), serpentine (7%), calcite (15%), talc (5%), chromite (2%), and goethite (1%). Dunite is light brownish grey to greenish in color and exhibits a holocrystalline texture with fine to coarse phaneritic grains. It is composed predominantly of olivine (92%), with minor pyroxene (3%), serpentine (3%), and iron oxides (2%). Similar to harzburgite, fractures are typically filled with silica and serpentine minerals. Microscopically, dunite displays fine to coarse grains comprising olivine (73%), orthopyroxene (10%), talc (15%), serpentine (1%), and magnetite (1%). Both rock units are part of the Cretaceous-aged Ultramafic Complex.

The structural geology of the area is dominated by a fault plane striking N 312° E with a dip of 80°, and an associated lineation trending 55°–N 320° E. The fault is classified as a right-lateral reverse slip fault and is interpreted as part of the Lawanopo fault system with dextral kinematics.

The lateritic profile in the Mandiodo Block is primarily derived from harzburgite. Vertically, the profile consists of a topsoil horizon averaging 1 meter thick, reddish-brown in color, clayey-sandy in texture, and characterized by the presence of hematite (15–30%), goethite (5%), and humic materials. The limonite zone can be subdivided into red limonite and

yellow limonite, with an average thickness of 13 meters. This zone contains goethite (15–30%), hematite (5%), manganese oxides, and quartz. The underlying saprolite zone is typically described as earthy to rocky saprolite, reddish-brown to greenish-brown in color, with an average thickness of 8.5 meters. It is composed of serpentine, goethite, hematite, manganese, garnierite, and quartz.

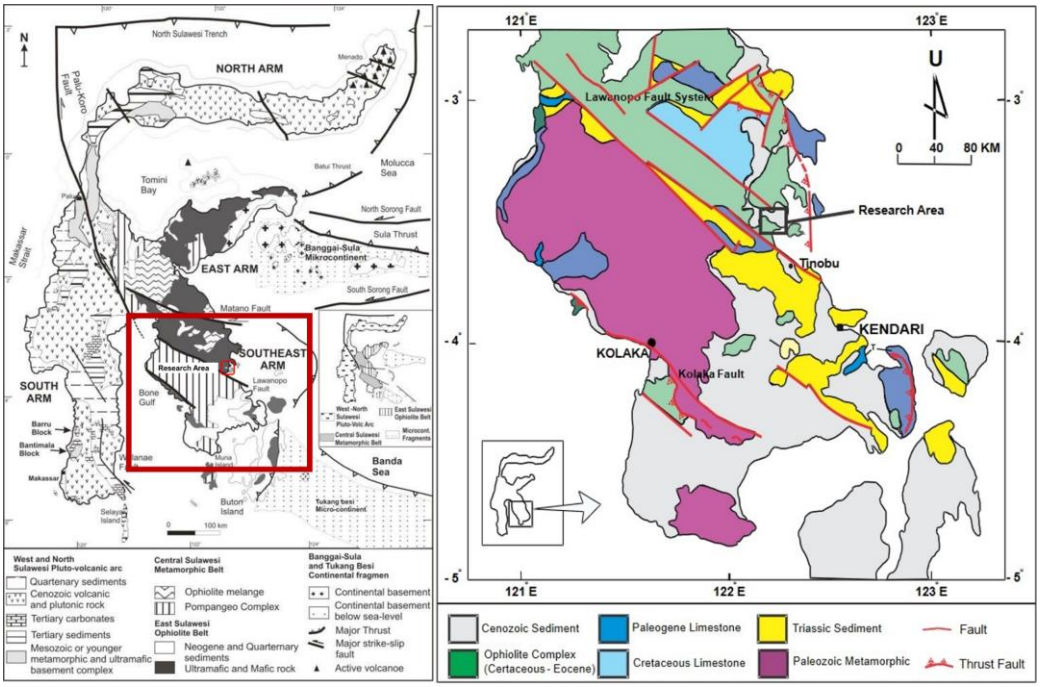

Figure 2.
Geological map of Sulawesi Tenggara Province, Surono [9] and location of Mandiodo Area on Ophiolite Complex.

Based on scandium research in North Konawe by Paskarino et al. [11], scandium enrichment is found in the limonite zone with controlling Fe_2O_3 and Al_2O_3 compounds, where favorable Fe_2O_3 grades are > 60%, while Al_2O_3 is > 7%. However, it is not certain which minerals carry this element in bedrock and which minerals bind it in the enrichment zone. The Mandiodo area has a limonite zone with Fe_2O_3 grades up to 70% and Al_2O_3 grades up to 8% (unreported data), which is interpreted to also contain high-grade scandium in the limonite.
Therefore, this study aims to determine the presence and characteristics of scandium enrichment in the Mandiodo nickel laterite area, as well as to identify the scandium-bearing minerals in the bedrock.

2. Sample and Methods

The samples used in this study included laterite zone pulp samples and bedrock cores from three drill holes conducted in the research area. The pulp samples weighed 100 grams each, with a 200-mesh size, collected from each meter of the drill holes, totaling 72 samples. The bedrock core samples were obtained from the deepest depths of each drillhole to minimize weathering effects, with a total of three samples from three drillholes.

Pulp samples were used to analyze the geochemistry and mineralogy of the laterite zone, where all 50 grams of pulp samples were used for Analytical Spectral Devices (ASD) to determine hydrous minerals on the laterite profile and X-Ray Fluorescence (XRF) analysis to determine the major elements in the samples, namely Fe_2O_3, Al_2O_3, SiO_2, MgO, and TiO_2. From these results, laterite geochemical characteristics were grouped, which became the basis for composite samples at several depths to conduct Inductively Coupled Plasma (ICP-OES) and X-Ray Diffraction (XRD) analysis. In addition, the major element content of the XRF results is also used to calculate the grade of weathering using formula 1 (Ultra Mafic Index of Alteration) and element mobility using formula 2 [2].

$$\text{UMIA (\%)} = \frac{[\,Al_2O_3 + Fe_2O_3\ Grade]}{[\,Al_2O_3 + MgO + SiO_2 + Fe_2O_3\ Grade]} \times 100\% \quad (1)$$

$$\text{Mobility } (\tau_{i,j}) = \frac{Cj,w \times Ci,p}{Cj,p \times Ci,w} - 1 \quad (2)$$

Where $\tau_{i,j}$ is the mass transfer coefficient of element j with respect to i, C is the grade, j is the measured element, i is immobile, p is protolith, and w is weathered. $C_{j,w}$ is the grade of element j in the laterite, and $C_{j,p}$ is the grade of element j in the original rock.

- $\tau_{i,j} = -1$, element j has been fully mobilized from the bedrock
- $-1 < \tau_{i,j} < 0$, there is partial mobilization of element j due to the weathering process
- $0 < \tau_{i,j} < 1$, there is an addition or enrichment of element j in weathering

ICP-OES is used to determine scandium grade using 50 grams of composite samples, while XRD is employed to analyze the mineralogical content in the laterite zone using 50 grams of composite samples. The list of composite samples can be found in Table 1. Core samples were utilized for two analyses: petrography-mineralogy and Scanning Electron Microscopy-Energy Dispersive X-Ray (SEM-EDX). Petrography and mineralogy were used to identify mineral names, rock genesis, and the presence of metallic minerals in the bedrock, while SEM-EDX was used to determine which scandium-bearing minerals are present in the bedrock.

Table 1.
Pulp sample used on this study.

Drillhole	Total Sample	Composite Sample	Composite Sample Count
O1	34	Topsoil (0-1 m), Limonite 1 (4-12m), Limonite 2 (12-20m), Saprolite (20-30m), Bedrock (30-32m)	5
O2	15	Topsoil (0-6m), Limonite (6-7m), Saprolite (7-11.5m), Bedrock (11.5-14m)	4
O3	23	Topsoil (0-1 m), Limonite 1 (1-2m), Limonite 2 (2-16m), Saprolite (16-18.5m), Bedrock (18.5-21.5m)	5

The results of these analyses were then compiled in laterite profiles, geochemistry, mineralogy, degree of weathering, and element mobility that were used to determine the characteristics of scandium enrichment, including enrichment zones, grade, controlling elements, mineralogy, relationships with elemental mobility, and rock weathering. In addition, the scandium content by SEM, combined with petrographic-mineralogical results, was used to identify the scandium-bearing minerals in bedrock.

3. Result & Discussion

3.1. Laboratory Result

The results of the XRF, ICP-OES, weathering rate and mobility analyses are presented in Table 2 the XRD results are shown in Table 3 and the ASD results are shown in Table 4.

Table 2.
XRF, ICP-OES, UMIA< and mobility result.

Drillhole O1											
	Depth (m)	**Sc (ppm)**	**Ni (%)**	**Fe (%)**	**Fe_2O_3 (%)**	**Al_2O_3 (%)**	**MgO (%)**	**SiO_2 (%)**	**TiO_2 (%)**	**UMIA**	**Mobility of Sc**
Topsoil	0-4	-	1.15	44.29	63.27	13.32	0.64	1.57	0.15	93.26	-
Limonite	4-12	95	1.33	42.78	61.11	13.15	0.84	3.15	0.11	88.73	-0.1730
Limonite	12-20	89	1.45	31.15	44.51	9.10	6.16	22.49	0.10	44.70	-0.2015
Saprolite	20-30	16	0.81	7.56	10.79	2.02	31.71	40.32	0.02	6.31	-0.2492
Bedrock	30-32	13	0.34	6.06	8.66	1.45	34.67	41.56	0.01	4.65	0
Drillhole O2											
	Depth (m)	Sc (ppm)	Ni (%)	Fe (%)	Fe_2O_3 (%)	Al_2O_3 (%)	MgO (%)	SiO_2 (%)	TiO_2 (%)	UMIA	Mobility of Sc
Topsoil	0-6	-	1.27	62.21	43.55	8.42	3.14	5.78	0.09	75.31	-
Limonite	6-7	70	1.23	52.08	52.08	4.67	4.38	22.19	0.06	46.57	-0.1131
Saprolite	7-11.5	43	1.10	36.54	36.54	4.29	14.01	26.71	0.05	30.81	-0.3478
Bedrock	11.5-	13	0.24	8.98	8.98	1.49	38.03	39.05	0.005	4.69	0
Drillhole O3											
	Depth (m)	Sc (ppm)	Ni (%)	Fe (%)	Fe_2O_3 (%)	Al_2O_3 (%)	MgO (%)	SiO_2 (%)	TiO_2 (%)	UMIA	Mobility of Sc
Topsoil	0-1	-	0.64	42.99	61.41	13.46	2.45	4.66	0.28	80.42	-
Limonite	1-2	104	1.01	46.62	66.59	9.95	1.47	2.39	0.14	88.21	-0.4471
Limonite	2-16	100	1.15	44.33	63.33	8.79	3.00	5.46	0.08	76.72	-0.1131
Saprolite	16-	51	1.27	29.39	41.98	5.06	14.51	21.72	0.05	34.98	-0.1334
Bedrock	18.5-21.5	11	0.26	5.91	8.45	1.17	41.17	38.45	0.006	4.12	0

Table 3.
XRD result of this study.

Drillhole O1

Minerals	Limonite (%)		Saprolite (%)	Bedrock (%)	Chemical Composition
	0-4m	4-12m	12-20m	20-30m	
Goethite	5.39	9.44	9.74	2.44	$FeO(OH)$
Talc-1A	44.99	21.9	1.37	5.93	$Mg_3(Si_2O_5)_2(OH)$
Gypsum	49.62	-	-	-	$Ca(SO_4)(H2O)_2$
Enstatite Fe 2+ bearing	-	11.87	7.33	14.56	$(Mg.\ Fe)SiO_3$
Forsterite, Syn	-	15.64	13.36	48.96	Mg_2SiO_4
Clinochlore-1A	-	8.29	29.98	13.61	$Mg_{2.3}Cr_{0.1}Fe_{0.1}Al_{1.2}Si_{1.3}O_5(OH)_4$
Vermiculite-2M	-	16.22			$Mg_3(Si_4O_{10})(OH)_2$
Magnesio-hornblende	-	14.35	4.31	5.13	$Ca_2(Mg_4Al)(Si_7Al)O_{22}(OH)_2$
Lizardite-1T	-	0.97	14.31	5.4	$Mg_3Si_2O_5(OH)_4$
Illite (NR)	-	-	3.54	-	$K_{0.78}Mg_{0.18}Ti_{0.01}Al_{2.46}Si_{3.36}O_{10}(OH)_2$
Gibbsite, Syn	-	1.97	4.98	3.96	$Al(OH)_3$
Enstatite Fe 2+ bearing	-	-	-	-	$(Mg.Fe)SiO_3$
Pyrophanite, Mg-bearing, Syn	-	-	3.79	-	$Mg_{0.1}TiMn_{0.9}O_3$

Drillhole O2

Minerals	Limonite (%)	Saprolite (%)	Bedrock (%)	Chemical Composition
	6-7 m	7-11.5 m	11.5-14 m	
Goethite	14.26	5.55	-	$FeO(OH)$
Talc-1A	49.47	25.16	4.39	$Mg_3(Si_2O_5)_2(OH)$
Quartz, Syn	23.09	5.5	-	SiO_2
Groutite	8.86	-	-	$MnO(OH)$
Lithiophorite	4.33	-	-	$(Li,Al)Mn^{+4}O_2(OH)_2$
Enstatite Fe 2+ bearing	-	-	18.45	$(Mg,\ Fe)SiO_3$
Forsterite, Syn	-	21.24	72.57	Mg_2SiO_4
Clinochlore-1A	-	5.39	-	$Mg_{2.3}Cr_{0.1}Fe_{0.1}Al_{1.2}Si_{1.3}O_5(OH)_4$
Vermiculite-2M	-	9.32	-	$Mg_3(Si4O_{10})(OH)_2$
Magnesio-hornblende	-	9.31	2.42	$Ca_2(Mg_4Al)(Si_7Al)O_{22}(OH)_2$
Lizardite-1T	-	1.76	2.58	$Mg_3Si_2O_5(OH)_4$
Illite (NR)	-	-	-	$K_{0.78}Mg_{0.18}Ti_{0.01}Al_{2.46}Si_{3.36}O_{10}(OH)_2$
Gibbsite, Syn	-	-	-	Al(OH)3
Enstatite Fe 2+ bearing	-	17.88	-	$(Mg,\ Fe)SiO_3$
Pyrophanite, Mg-bearing, Syn	-	-	-	$Mg_{0.1}TiMn_{0.9}O_3$

Drillhole O3

Minerals	Limonite (%)		Saprolite (%)	Bedrock (%)	Chemical Composition
	1-2m	2-16m	16-18.5m	18.5-21.5m	
Goethite	76.86	24.47	16.83	-	$FeO(OH)$
Talc-1A	23.14	45.89	39.43	12.67	$Mg_3(Si_2O_5)_2(OH)$
Groutite	-	10.03	-	-	$MnO(OH)$
Lithiophorite	-	7.53	-	-	$(Li,Al)Mn^{+4}O_2(OH)_2$

Enstatite Fe 2+ bearing	-	-	-	16.49	$(Mg, Fe)SiO_3$
Forsterite, Syn	-	-	-	36.78	Mg_2SiO_4
Clinochlore-1A	-	-	3.52	-	$Mg_{2.3}Cr_{0.1}Fe_{0.1}Al_{1.2}Si_{1.3}O_5(OH)_4$
Vermiculite-2M	-	-	8.48	-	$Mg_3(Si_4O_{10})(OH)_2$
Magnesio-hornblende	-	-	9.48	1.66	$Ca_2(Mg_4Al)(Si_7Al)O_{22}(OH)_2$
Lizardite-1T	-	-	19.71	13.47	Mg3Si2O5(OH)4
Illite (NR)	-	-	-	-	$K_{0.78}Mg_{0.18}Ti_{0.01}Al_{2.46}Si_{3.36}O_{10}(OH)_2$
Gibbsite, Syn	-	12.08	3.11	-	$Al(OH)_3$
Apophyllite-(KF)	-	-	-	13.47	$KCa_4F(Si_2O_5)_4.8H_2O$

Table 4.
ASD result of this study.

Drillhole O1					
Depth (m)	**Fe Oxide**	**Clay Minerals**	**Depth (m)**	**Fe Oxide**	**Clay Minerals**
1		-	18	-	-
2	-	-	19	-	Chlorite
3	-	-	20	-	Chlorite
4	-	Gibbsite	21	-	Antigorite
5	-	-	22	Goethite	Antigorite
6	-	-	23	-	Antigorite
7	-	-	24	-	Antigorite
8	-	-	24,5	-	Antigorite
9	-	-	25	-	Antigorite
10	-	-	26	Goethite	Antigorite
11	Goethite	Gibbsite	27	Goethite	Antigorite
12	-	Gibbsite	27,6	-	Antigorite
13	-	Chlorite	28	-	Antigorite
14	-	-	29	Goethite	Antigorite
15	-	-	30	Goethite	Antigorite
16	-	-	31	-	Antigorite
17	-		32	-	Antigorite
Drillhole O2					
Depth (m)	Fe Oxide	Clay Minerals	Depth (m)	Fe Oxide	Clay Minerals
1	Goethite	-	9	goethite	
2	Goethite	-	10	goethite	
3	Goethite	-	11	goethite	Chlorite
4	Goethite	gibbsite	11,5	goethite	Chlorite
5	Goethite	-	12	-	Chlorite
6	Goethite	-	13	-	Chlorite
7	Goethite	-	14	-	Chlorite
8	Goethite	talc			Chlorite
Drillhole O3					
Depth (m)	Fe Oxide	Clay Minerals	Depth (m)	Fe Oxide	Clay Minerals
1	Goethite	-	13	Goethite	-
2	Goethite	-	14	Goethite	-
3	Goethite	-	15	Goethite	-
4	Goethite	-	16	Goethite	-
5	Goethite	-	17	Goethite	Antigorite
6	Goethite	-	18	Goethite	Antigorite
7	Goethite	-	18.5	Goethite	-
8	Goethite	-	19	-	Serpentine
9	Goethite	-	20	-	Serpentine
10	Goethite	-	21	-	Serpentine
11	Goethite	-	21.5	-	Serpentine
12	Goethite	-	-	-	-

3.2. Drillhole Analysis

3.2.1. Drillhole O1

A summary of the results of the O1 drillhole analysis is presented in the laterite, geochemistry, mineralogy, UMIA and Mobility profiles in Figure 3.

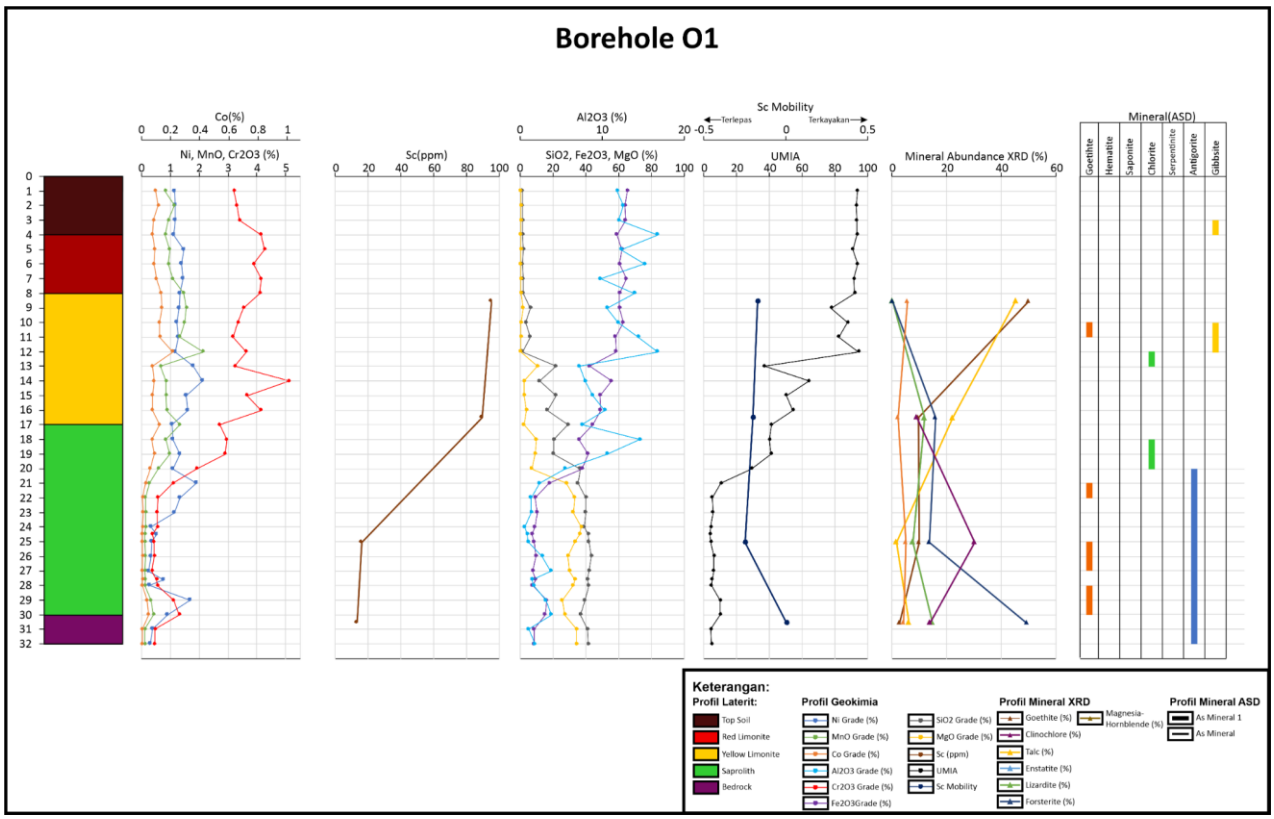

Figure 3.
Laterite, geochemistry, mineralogy, UMIA, and mobility profile of O1 drillhole.

3.2.1.1. Topsoil Zone

The nickel laterite of drillhole O1 shows 4 meters of topsoil thickness with SiO_2 (1.66%), MgO (0.6375%), Fe_2O_3 (63.27%), Al_2O_3 (13.31%), and Ni (1.15%), containing hematite (10-30%), goethite (20%), manganese (0.5%), and the presence of the mineral gibbsite.

3.2.1.2. Limonite Zone

The limonite zone can be divided into a four-meter red limonite layer and a nine-meter yellow limonite layer. Red limonite contains goethite, hematite, and manganese. In yellow limonite, goethite (9.44%-49.62%), talc (21.9%-44.99%), chlorite (1%), gibbsite (3.7%), enstatite (11.68%), forsterite (15.64%), vermiculite (16.22%), Mg-hornblende (15.35%), and clinochlore (8.82%) were identified. The average SiO_2 content of 29.45% shows a stable pattern with increasing depth, with low values in the red limonite section and an increase in the yellow limonite. The average grade of MgO (1.55%) and Fe_2O_3 (57.24%) remains stable in red limonite and then decreases in yellow limonite. The Al_2O_3 grade of 11.66 ppm fluctuates, and Ni grade at a depth of 14 meters reaches 2.13%. The average SiO_2 content remains around 29.45%, with low values in the red limonite and an increase in the yellow limonite. The average MgO content is 1.55%, and Fe_2O_3 is 57.24%, with a stable pattern in red limonite and a decrease in yellow limonite. The Al_2O_3 content averages 11.66% with a fluctuating pattern, and Ni content is 1.4%, reaching a maximum of 2.13% at 14 meters depth.

3.2.1.3. Saprolite Zone

The saprolite zone has 13 meters of thickness and contains serpentine, chlorite, antigorite, goethite (9.74%), talc (1.37%), gibbsite (4.98%), enstatite (7.33%), lizardite (4.31%), forsterite (13.35%), Mg-hornblende (4.31%), clinochlore (29.98%), and illite (3.54%). The average SiO_2 content is 36.48%, MgO is 26.12%, Fe_2O_3 is 17.97%, Al_2O_3 is 3.89%, and Ni content fluctuates with increasing depth, reaching a maximum grade of 1.89 ppm at 20 meters depth.

3.2.1.4. Bedrock

Thin section and polished samples exhibit a holocrystalline texture, medium-coarse phaneritic, hypidiomorphic equigranular, with olivine (68.01%), orthopyroxene (27.5%), clinopyroxene (0.57%), spinel (0.77%), serpentine (1.15%), magnetite (2%), and pyrite (rare). XRD analyses of the bedrock indicate a composition of forsterite (48.92%), enstatite (14.56%), lizardite (5.39%), clinochlore (3.61%), and talc (5.93%). The olivine identified from the thin section is forsterite, pyroxene is enstatite, and serpentine is lizardite. Based on Streckeisen [12] classification: The O1 bedrock is classified as

harsburgite, characterized by a greenish-grey color, hardness, slight weathering, low serpentinization, medium fracturing, with serpentine content reaching 5%. The average SiO_2 content increased to 42.55%, MgO to 34.67%, Fe_2O_3 decreased to 8.65%, Al_2O_3 decreased to 1.45%, and Ni decreased to 0.34%.

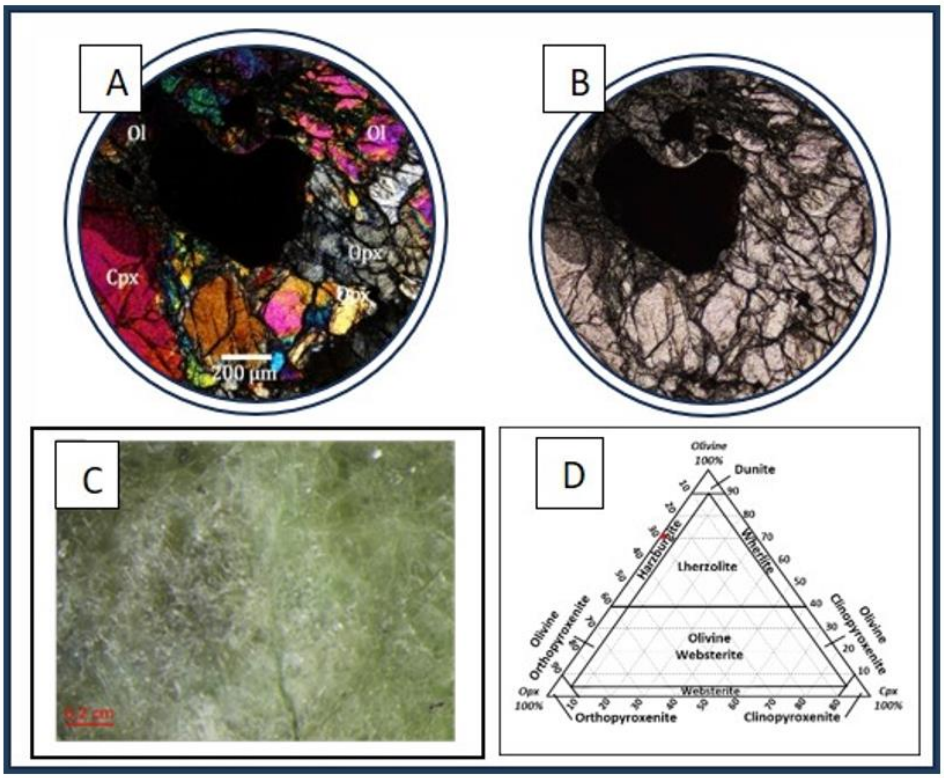

Figure 4.
Photograph of bedrock O1: (a) Thin section on PPL, (b) Thin section on XPL, (c) Binocular photograph, (d) Rock classification result Streckeisen [12].

3.2.1.5. Weathering Process Intensity

The weathering rate was calculated quantitatively using the UMIA formula, with the results shown in the UMIA profile against depth. Weathering rates have values that increase as depth decreases. In the bedrock, the average UMIA value is 0.04, then increases in the saprolite zone to 0.15, then in the limonite to 0.76, and in the overburden zone to 0.93, which is the highest value. Scandium grades have a similar trend to UMIA and therefore are visually positively correlated.

3.2.1.6. Scandium Enrichment

Scandium grade increases towards the top of the laterite and is enriched with the highest grade of 95 ppm in the limonite zone. Scandium grades are positively correlated with Fe_2O_3 and Al_2O_3. Additionally, the scandium content is positively correlated with goethite, which has the highest goethite content (=49%), and gibbsite in the scandium enrichment zone.

3.2.2. Drillhole O2

Drillhole O2 has 5,5 meters of laterite thickness of 14 meters total depth. The analysis results were summarized in the laterite, geochemistry, mineralogy, UMIA and mobility profiles in Figure 7.

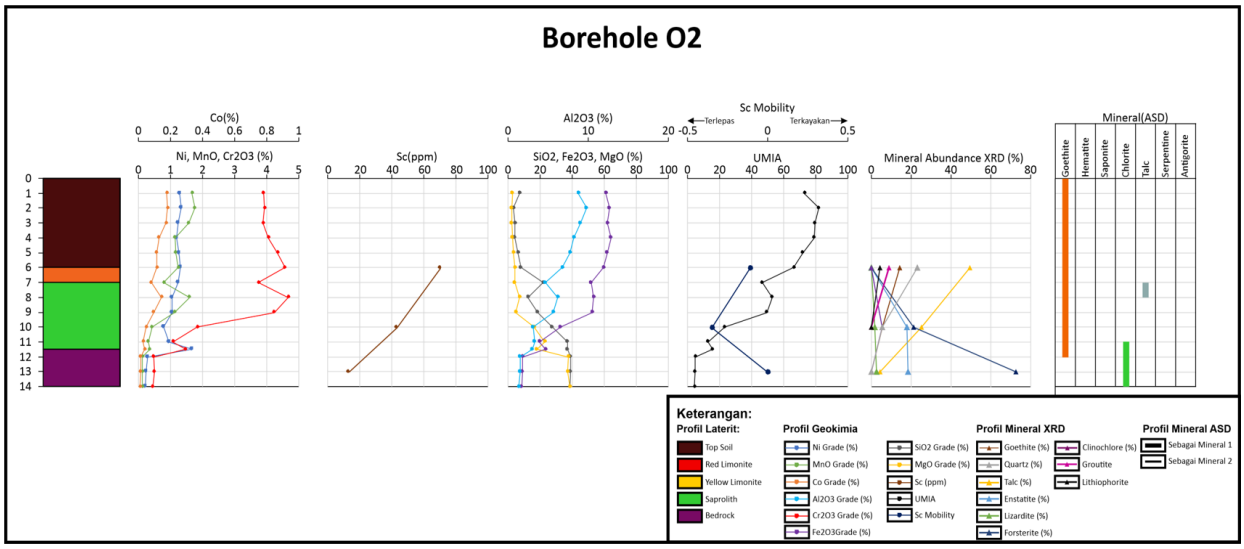

Figure 5.
Laterite, geochemistry, mineralogy, UMIA, and mobility profile of drillhole O2.

3.2.2.1. Topsoil Zone

The O2 drillhole profile shows 6 meters of topsoil thickness with SiO_2 (5.77%), MgO (3.135%), Fe_2O_3 (62.21%), Al_2O_3 (8.41%), and Ni (1.27%). This topsoil is descriptively reddish-brown, clayey, and contains hematite (10-30%), goethite (10-15%), and manganese (1%). ASD analysis results show the presence of goethite.

3.2.2.2. Limonite Zone

Yellow limonite, which is only one meter thick, has a yellow-brown color. The limonite zone features clay-sized particles, soft hardness, and contains goethite, hematite, and manganese. XRD results indicate the presence of goethite (16.82%), quartz (25.56%), and talc (57.68%). Meanwhile, ASD results confirm the presence of goethite. In this zone, the average SiO_2 content reaches 22.9%, MgO 4.38%, Fe_2O_3 52.08%, Al_2O_3 4.67%, and Ni 1.24%.

3.2.2.3. Saprolite Zone

The saprolite zone has a thickness of 4.5 meters. Descriptively, it has a clayey, friable grain size, soft to medium hardness, yellow-brown color, serpentine, and goethite composition. XRD results show the presence of goethite (5.55%), quartz (5.5%), talc (25.16%), enstatite (17.87%), lizardite (1.57%), forsterite (21.44%), vermiculite (9.32%), and clinochlore (5.3%). Meanwhile, the ASD results show the presence of goethite, talc, and chlorite minerals.

This zone has an average SiO_2 content of 26.21% and MgO (14.05%), which increase with depth, respectively, Fe_2O_3 (36.54%) and Al_2O_3 (4.29%), which decrease with depth, and an average Ni content of 1.1%, which fluctuates with depth and reaches a maximum of 1.67% at 11 meters at the bottom of the saprolite.

3.2.2.4. Bedrock

The original rock of the low-serpentinized harzburgite is composed of serpentine (5-15%), olivine (45-50%), and pyroxene (10-20%). In this zone, the average SiO_2 content is 39.04%, MgO is 38.02%, Fe_2O_3 is 8.98%, Al_2O_3 is 1.48%, and Ni is 0.24%. Petrographic and mineragraphic analyses reveal a holocrystalline texture, medium-coarse phaneritic, hypidiomorphic, and equigranular, with olivine (77.64%), orthopyroxene (13.7%), clinopyroxene (0.28%), spinel (5%), serpentine (1.63%), talc (0.25%), magnetite (1.5%), and pyrite (rare). XRD results of the bedrock indicate mineral composition includes forsterite (75.56%), enstatite (18.45%), lizardite (2.58%), and magnesio-hornblende (2.4%). Olivine identified from thin sections is forsterite, pyroxene is enstatite, and serpentine is lizardite. Based on Streckeisen [12] classification, the O2 bedrock is classified as harzburgite.

XRF results on the bedrock show the average SiO_2 increased to 39.04%, the average MgO content increased to 38.02%, the average Fe_2O_3 content decreased to 8.98%, the Al_2O_3 content decreased to 1.48%, and the Ni content decreased to 0.24%.

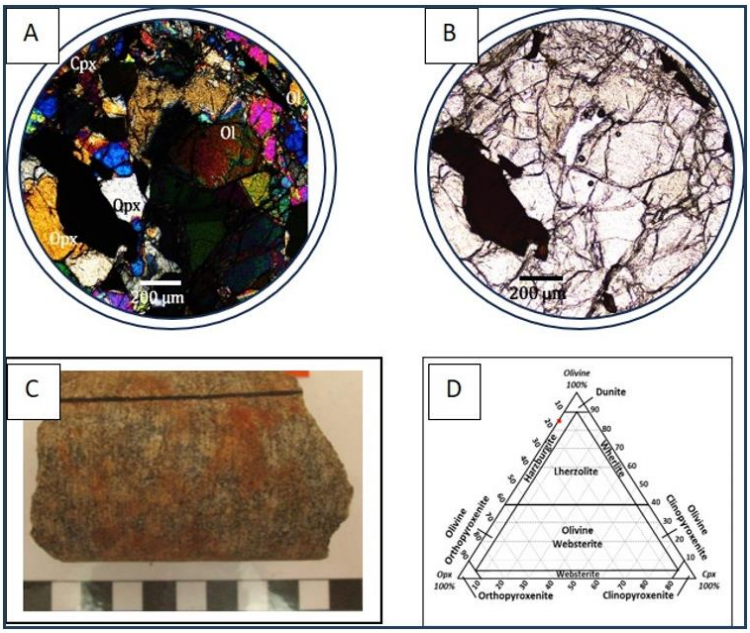

Figure 6.
Photographs of bedrock O2: (a) Thin section on PPL, (b) Thin section on XPL, (c) Binocular photographs, (d) Rock classification results Streckeisen [12].

3.2.2.5. Weathering Process Intensity (Ultramafic Index of Alteration)

The degree of weathering is calculated quantitatively using the UMIA formula with results that can be seen in the UMIA profile against depth. The weathering rate has an increasing value as the depth decreases. The average UMIA of bedrock is 0.04, then increases in the saprolite zone to 0.31, then increases in limonite to 0.46, increases again in the overburden zone to 0.75, and reaches a maximum of 0.81. Scandium grades have a trend that is visually positively correlated with UMIA.

3.2.2.6. Scandium Enrichment

Scandium grade increases towards the top of the drill hole, but there is no enrichment, as the highest grade is 70 ppm in the limonite zone. Scandium grades are visually positively correlated with Fe_2O_3 and Al_2O_3 grades. Additionally, scandium grade shows a visual positive correlation with goethite and talc, with the highest goethite (16.8%) and talc (57.68%) grades in the scandium enrichment zone. The ASD also indicates the presence of goethite mineral in the scandium enrichment zone.

3.2.3. Drillhole O3

This drillhole has a depth of 21.5 meters, with a laterite thickness of 17 meters. A summary of the results of the O3 drillhole analysis is presented in the sections on laterite, geochemistry, mineralogy, UMIA, and mobility profiles in Figure 11.

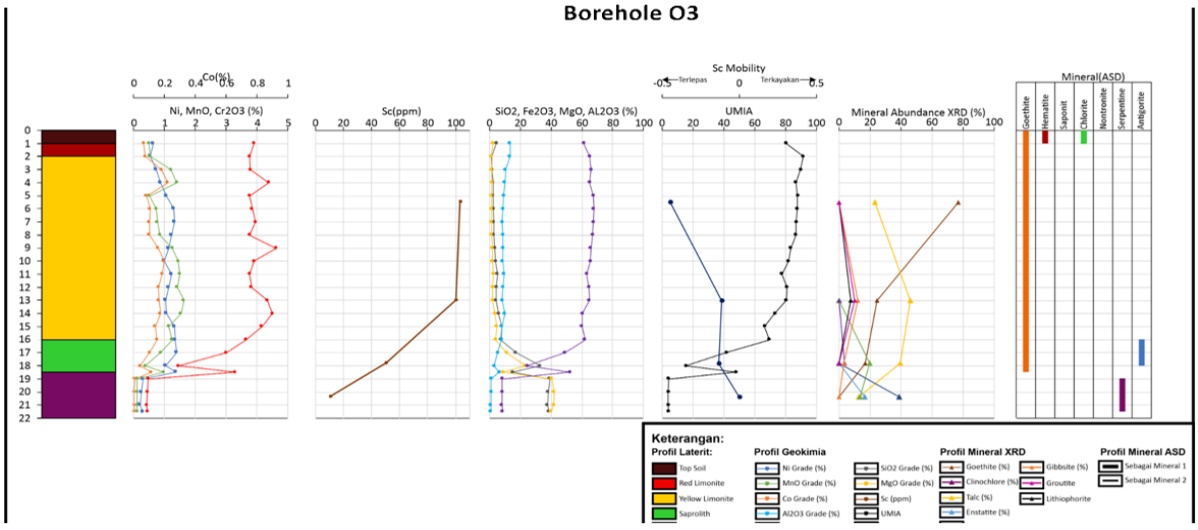

Figure 7.
Laterite, geochemistry, mineralogy, UMIA, and mobility profile of O3 drillhole.

3.2.3.1. Topsoil Zone

The O3 drillhole profile shows a topsoil thickness of 1 meter with SiO_2 (4.66%), MgO (2.45%), Fe_2O_3 (61.41%), Al_2O_3 (13.46%), and Ni (0.64%). This zone descriptively has a red-brown color, is clay-grained, and contains 20% hematite. ASD analysis results show the presence of goethite, hematite, and chlorite.

3.2.3.2. Limonite Zone

The limonite is 15 meters thick, consisting of 1 meter of red limonite and 14 meters of yellow limonite. Descriptively, the red limonite zone is reddish brown, and the yellow limonite is yellowish brown. It has a clay size, soft hardness, and contains goethite and hematite. XRD results show the presence of goethite (76.85%) in the upper part and (27.56%) in the lower limonite, talc (23.14%) in the upper part and (6.2%) in the lower part, and gibbsite (12.24%) in the lower part. Meanwhile, the ASD results also show the presence of goethite throughout the limonite zone.

In this zone, the SiO_2 content averages 4.02%, the MgO content averages 2.28%, the Fe_2O_3 content averages 64.85%, and the Al_2O_3 content averages 9.39%, which are stable with depth, while the Ni content of 1.08% is quite volatile, reaching 1.35% at 15 meters depth.

3.2.3.3. Saprolite Zone

The saprolite zone is 2 meters thick. Descriptively, it has a clay-sand grain size, soft hardness, yellowish-brown color, and contains serpentine and goethite. XRD results show the presence of goethite (16.83%), talc (39.41%), gibbsite (3.11%), lizardite (19.71%), and magnesia hornblende (9.48%). Meanwhile, the ASD results also show the presence of goethite and antigorite.

This zone has SiO_2 average (32.48%) and MgO average (14.51%) which increase with depth, Fe_2O_3 average (41.98%), Al_2O_3 average (5.06%) which decrease with depth, and Ni average (1.26%) which is quite stable against increasing depth and reaches a maximum at a depth of 11 meters with Ni (1.4%).

3.2.3.4. Bedrock

Bedrock of laterite is peridotite with blackish grey coloration, hard, slightly weathered, weakly serpentinized, containing serpentine (8-15%), olivine (35-40%), and pyroxene (10%). The grades of SiO_2 (38.44%) and MgO (41.16%) have increased, while the grades of Fe_2O_3 (8.48%), Al_2O_3 (1.17%), and Ni (0.29%) have decreased.

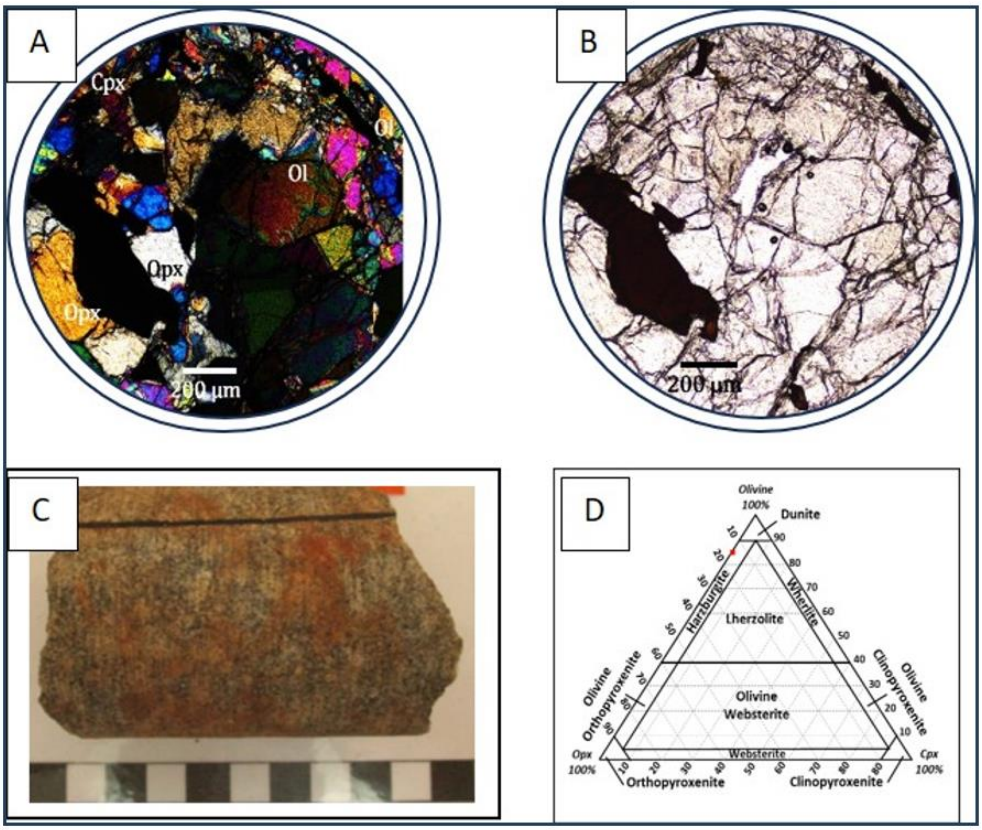

Figure 8.
Photo of O3 bedrock, (a) PPL appearance, (b) XPL appearance, (c) Hand specimen appearance, and (d) Ultramafic rock classification results Streckeisen [12].

3.2.3.5. Weathering Process Intensity (Ultramafic Index of Alteration)

Intensity of weathering is calculated quantitatively using the UMIA formula with results that can be seen in the UMIA profile against depth, and it would be increasing while the depth is decreasing. The average UMIA value of bedrock is 0.04,

then increases in the saprolite zone to 0.34, then increases in limonite to 0.82, and slightly decreases in the overburden to 0.80. Scandium grades reach their highest values at high UMIA values and appear to be positively correlated.

3.2.3.6. Scandium Enrichment

Scandium grades increase towards the top of the drill hole, but there is no enrichment, as the highest grade is 104 ppm in the limonite zone. Scandium grades are positively correlated with Fe_2O_3 and Al_2O_3 grades. Scandium is positively correlated with goethite and talc, with the highest goethite content (76.85%) in the scandium enrichment zone.

ASD results also show the presence of goethite minerals in the scandium enrichment zone. Scandium grades are positively correlated with Fe_2O_3 and Al_2O_3, as well as with goethite and talc, with the highest goethite content (76.85%) in the scandium enrichment zone. ASD also shows the presence of goethite mineral.

3.3. Scandium Enrichment Characteristics

Scandium is enriched in the upper limonite zone at a depth of 1-15 meters, with an average scandium enrichment of 92.25 ppm and a maximum grade of 104 ppm. Scandium is only enriched in the upper part of the laterite, indicating limited scandium mobility.

Scandium correlates with Fe, Cr, Al, Mn, and Co, showing similar scandium mobility to Fe, Cr, and Al, which are immobile. This indicates that the minerals binding scandium have a relationship with Fe, Al, Mn, Co, or Cr. Conversely, with magnesium (Mg), scandium is negatively correlated, indicating that Mg has very high mobility. Scandium is enriched as a residual deposit or leaching residue, positioned at the top of the laterite profile or in the yellow limonite, which is controlled by Fe_2O_3, Al_2O_3, and Cr_2O_3.

Table 5.
Correlation matrix of Sc, Fe, Al, Ni, Mn, Mg, and Cr.

	Sc_ppm	Fe_ppm	Al_ppm	Ni_ppm	Mn_ppm	Mg_ppm	Cr_ppm
Sc_ppm	1	0.97676	0.9401	0.785019	0.931843	-0.97965	0.99287
Fe_ppm	0.97676	1	0.884416	0.790958	0.941948	-0.97803	0.981021
Al_ppm	0.9401	0.884416	1	0.711866	0.889209	-0.89649	0.905827
Ni_ppm	0.785019	0.790958	0.711866	1	0.826868	-0.80449	0.826752
Mn_ppm	0.931843	0.941948	0.889209	0.826868	1	-0.92086	0.944975
Mg_ppm	-0.97965	-0.97803	-0.89649	-0.80449	-0.92086	1	-0.97969
Cr_ppm	0.99287	0.981021	0.905827	0.826752	0.944975	-0.97969	1

From a mineralogical perspective, ASD results show limited hydroxide minerals, consisting of goethite (FeO(OH)) and hematite (Fe_2O_3), in the enrichment zone, namely the upper limonite. Both of these minerals are Fe oxides that control scandium enrichment, thus strengthening the interpretation that these two minerals can bind scandium in the limonite zone.

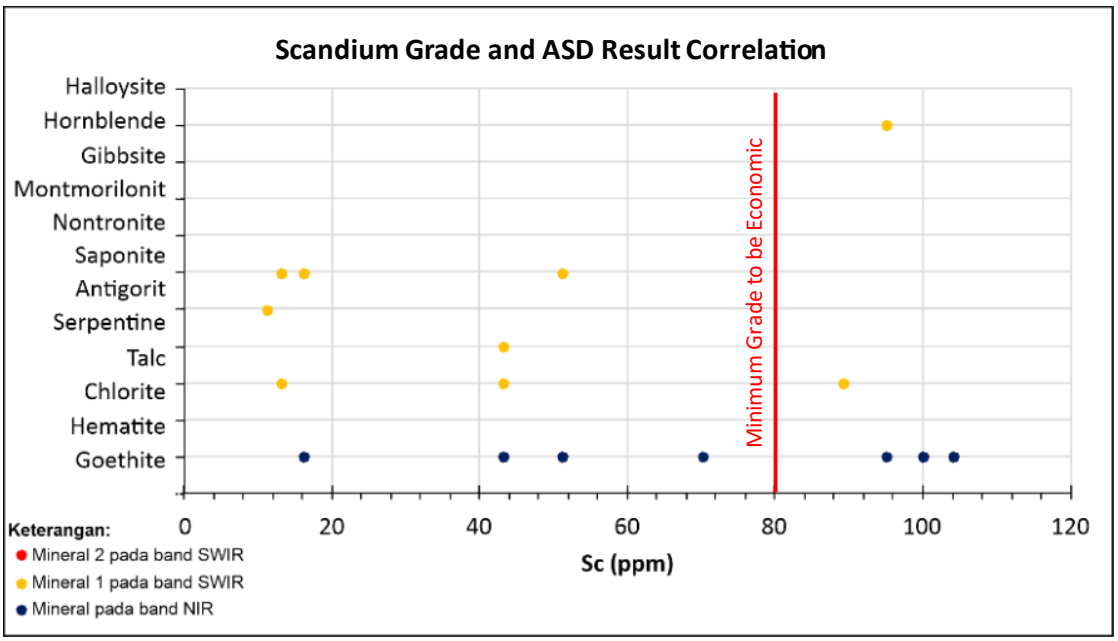

Figure 9.
Scandium correlation to ASD mineral.

Meanwhile, XRD results show that in the scandium enrichment zone, the minerals that appear in all drillholes are goethite (FeO(OH)) and talc ($Mg_3(Si_2O_5)_2(OH)$), which have an identical pattern to the fluctuations of scandium in the laterite profile. This reinforces the previous interpretation that goethite binds scandium, but the presence of talc is still not

well explained, especially since its constituents are negatively correlated with scandium. The behavior of goethite, which adsorbs metals easily, such as nickel, cobalt, copper, scandium, etc., is controlled by the large surface area of goethite, which results in good adsorption capacity [13].

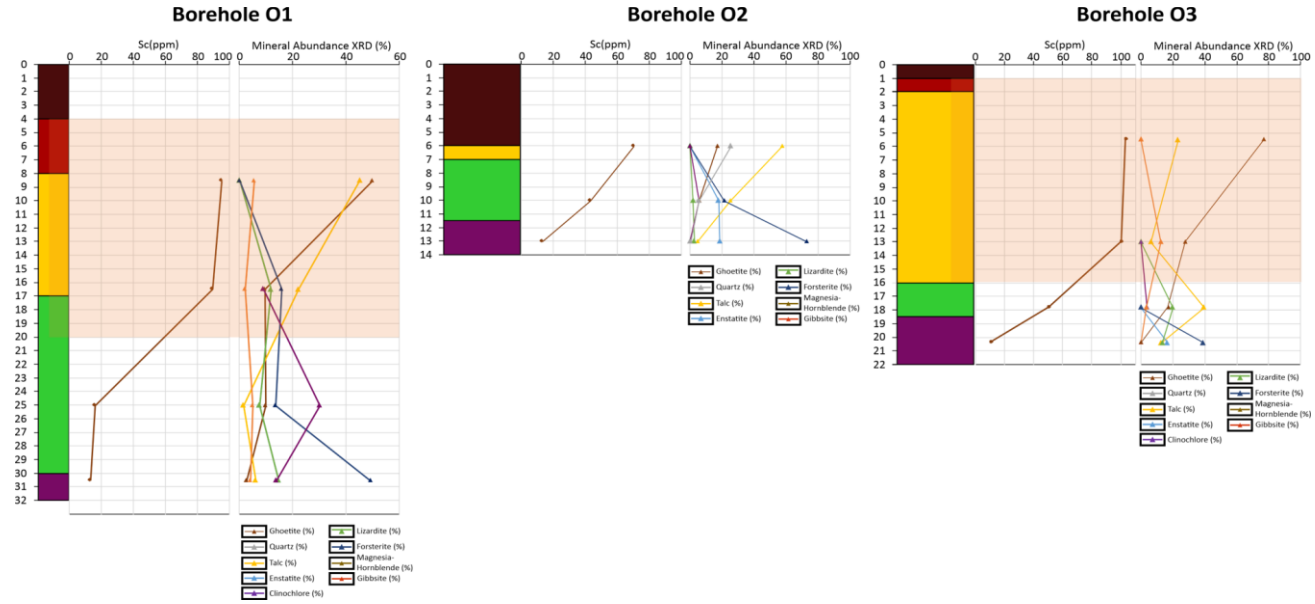

Figure 10.
Scandium and XRD result correlation.

As shown on nickel laterite profiles, particularly within the limonitic zone, increasing scandium concentrations are commonly associated with the presence of goethite, hematite, and low concentrations of chlorite and talc. Scandium displays a negative correlation with magnesium, indicating that scandium does not substitute for Mg in the crystal lattice but is rather enriched through different geochemical mechanisms. Conversely, a positive correlation between scandium and iron suggests that scandium is not incorporated through isomorphous substitution but is instead adsorbed onto Fe-bearing mineral phases, specifically goethite and hematite.

Laterite is characterized by a dominance of iron and oxygen elements, confirming the mineralogical presence of goethite. Spectral mapping reveals a notable surface concentration of scandium across these iron oxide minerals, further supporting its mode of occurrence as adsorbed ions on Fe-oxide surfaces rather than as structural components within silicate phases.

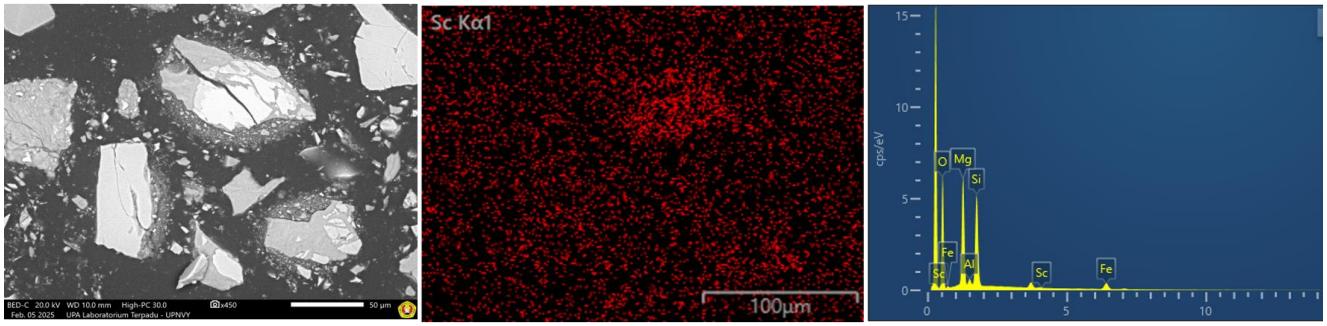

Figure 11.
(a) Limonite section from sample O2 embedded in resin, (b) Elemental spectrum of the observed area, (c) Elemental spectrum of the observed area.

Table 6.
Elemental composition derived from SEM mapping.

Element	Weight Percentage (% wt)	Element	Weight Percentage (% wt)	Element	Weight Percentage (% wt)	Element	Weight Percentage (% wt)
O	46.24	Al	1.32	Ca	9.69	Fe	4.12
Mg	16.13	Si	22.43	Sc	0.07		

3.4. Scandium in Bedrock

Scandium was detected within grain minerals in polished thin sections (Figure 18), co-occurring predominantly with calcium. Conversely, elements such as iron, silicon, chromium, oxygen, magnesium, and aluminum were present only in

trace amounts (Figure 18). Scandium appears to occupy microfractures within the host minerals, and scanning color spectrum analysis indicates that scandium is present at relatively high concentrations. According to the elemental composition data obtained from SEM mapping (Table 7), the scandium-hosting minerals in the primary rock are composed of calcium, magnesium, silicon, oxygen, and aluminum ($CaMgAlSiO_4$), suggesting a mixed silicate phase as the carrier.

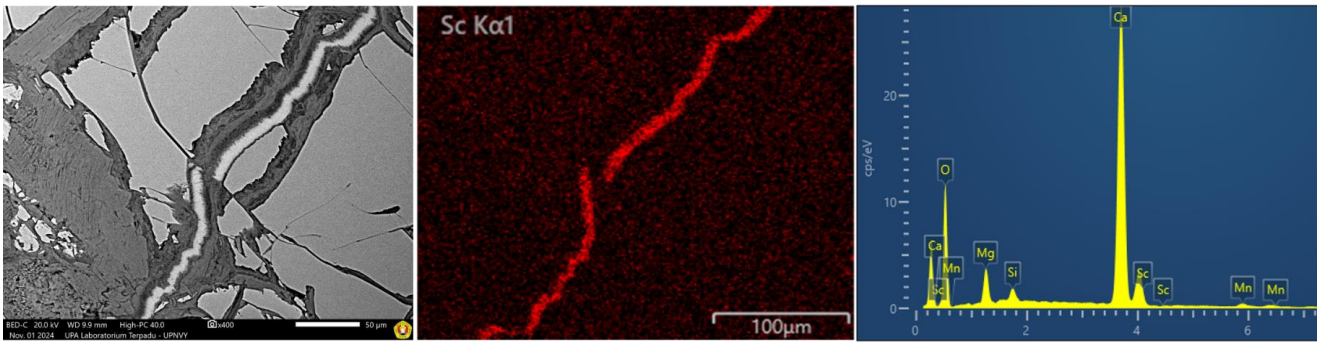

Figure 12.
(a) Polished section of sample O2, (b) SEM observation area, (c) Elemental spectrum of the observed area.

Table 1.
Elemental composition obtained from SEM-EDS mapping.

Element	Weight Percentage (% wt)	Element	Weight Percentage (% wt)
O	54.96	Ca	39.20
Mg	3.60	Sc	0.37
Si	0.94	Mn	0.93

Optical microscopy reveals the occurrence of clinopyroxene in the form of augite, exhibiting a distinction of lamellar texture characterized by the intergrowth of augite and diopside. Augite displays a parallel extinction pattern along the C-axis and appears bright under crossed nicols, whereas diopside, with its short-wave extinction, appears dark when augite is illuminated. The lamellar texture is interpreted as a product of exsolution during crystallization, driven by temperature and fluctuations in aluminum content during the formation of augite and diopside.

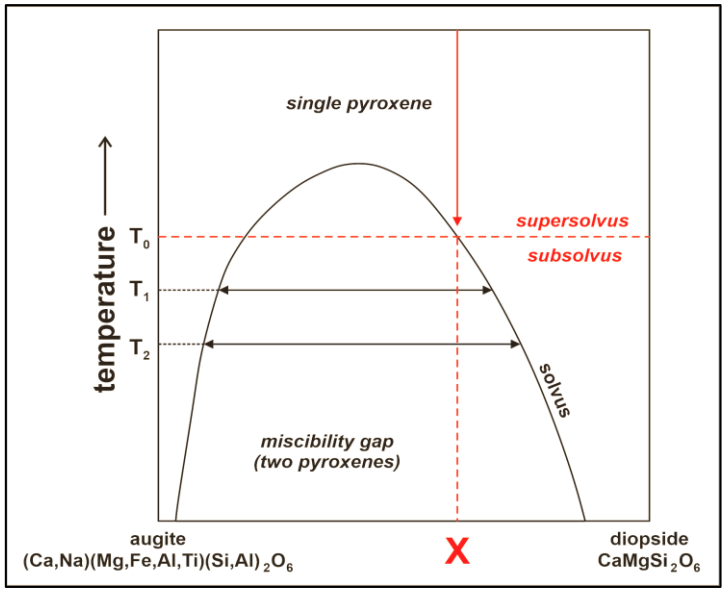

Figure 13.
Schematic diagram illustrating the formation of lamellar texture because of decreasing temperature in the magmatic solution (modified from Perkins D. et al [1])

The presence of lamellar textures in augite underscores the geochemical role of aluminum in its crystallization. Furthermore, the consistent association of aluminum with scandium in these pyroxene phases suggests that aluminum-rich augite serves as a primary host for scandium in the protolith. This mineralogical relationship reinforces the hypothesis that scandium partitioning during magmatic differentiation is closely linked to aluminum-bearing silicate phases. Pointing on lamellar texture using scanning electron microscopy shows the existence of scandium in the augite, which consists of calcium, sodium, magnesium, iron, aluminium, and silicon (Figure 21).

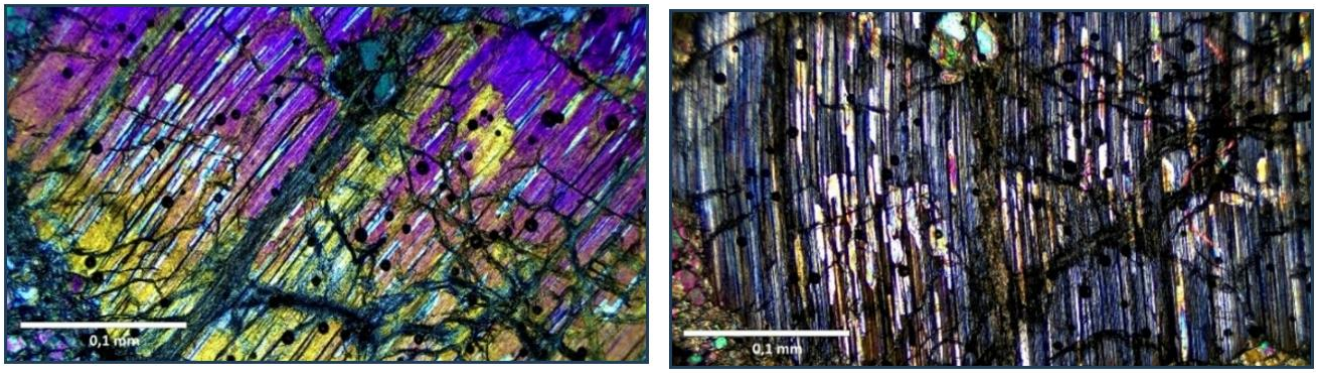

Figure 14.
Photomicrographs of augite in thin section under crossed polars: (left) length slow position and (right) length fast position.

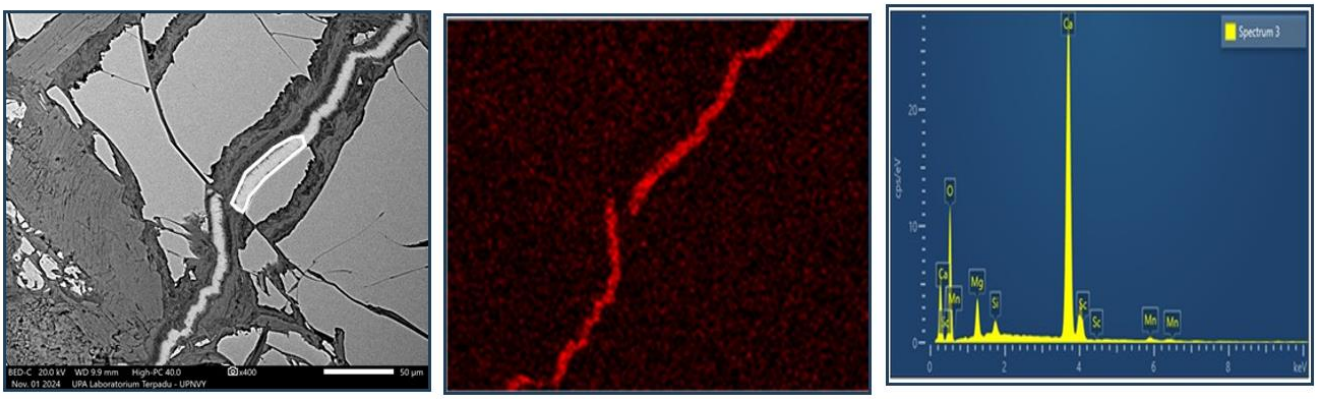

Figure 15.
SEM mapping on lamellar texture in augite and diopside shows scandium content in augite.

3.5. Scandium Weathering and Enrichment

Scandium tends to ionize and release electrons to form the trivalent cation Sc^{3+} under various physicochemical conditions that disrupt its geochemical stability. These conditions include changes in pH, temperature, and pressure, redox environments, and weathering processes. Weathering fundamentally involves the incorporation of oxygen into mineral crystal structures, which destabilizes scandium's original bonding configuration. As a result, scandium is mobilized from its primary host phase, becoming available to form new chemical associations in pursuit of a more stable geochemical state.
Several key environmental and geological conditions are required to develop lateritic nickel deposits systems:

1) Prolonged tectonic stability allows for the development of thick lateritic profiles over geological timescales (typically 1–6 million years) without significant erosion. In the study area, tectonic evolution began during the Cretaceous period (145–100 Ma), culminating in the emplacement of the ultramafic complex during the Middle Miocene (~15 Ma).
2) Moderate topographic relief, resulting from tectonic quiescence, enables effective chemical weathering. In this setting, the downward progression of weathering outpaces the surface lowering due to erosion and subsidence. These conditions promote optimal leaching of mobile elements from primary minerals.
3) A humid tropical climate with elevated temperatures accelerates laterization. The post-obduction Tampakura Formation in Southeast Sulawesi, interpreted as having developed under a tropical wet climate [9], confirms that the region has been situated in a tropical climatic zone since the emplacement of the ultramafic complex.
4) Vegetation plays a critical role by supplying organic matter and organic acids (e.g., humic, fulvic, oxalic, and lichenic acids), which enhance weathering rates. Decomposition of plant material produces acids that promote the breakdown of primary silicates and create reducing conditions. These conditions lead to the mobilization of ferric iron (Fe^{3+}) into soluble ferrous iron (Fe^{2+}), which later reprecipitates as iron oxides upon reoxidation.
5) Structural features, including joints and faults (both tectonic and cooling-induced), increase porosity in ultramafic rocks, enhance water infiltration, and accelerate laterization [14]. In the study area, extensive thrust faults and fracture systems associated with ophiolite uplift facilitate intensive weathering and laterite formation (Surono, 2013).
6) Soil acidity, driven by the rapid decomposition of organic matter and microbial activity, limits the development of thick humus layers and increases organic acid production. Furthermore, carbon dioxide released from organic decay combines with groundwater to form carbonic acid, further acidifying the soil and intensifying chemical weathering [14].

7) High annual rainfall, exceeding 1,800 mm, optimizes laterization. Under such conditions, highly leached and persistently moist soils form, typically between latitudes 5°–10° and 25° [14-16]**.** Rainfall above 1,500 mm/year is associated with the formation of gibbsite and kaolinite due to intense leaching [14, 17, 18]. The Tampakura Formation, postdating the ophiolite uplift, is consistent with these humid tropical conditions [9]. Meteorological data from the Indonesian Agency for Meteorology, Climatology, and Geophysics indicate that the average annual rainfall in North Konawe from 1991 to 2020 was approximately 2,295 mm, supporting sustained and intensive laterization processes in the region.

Laterite profiles in the Mandiodo area exhibit thicknesses ranging from 5.5 to 26 meters, with weathering intensity indices of 0.06 in the saprolite zone and 0.88 in the limonite zone, indicating moderate weathering.

4. Conclusion

Scandium enrichment in Mandiodo occurs in the limonite zone, with scandium grades reaching 104 ppm. This deposit is residual, associated with Fe_2O_3, Al_2O_3, and Cr_2O_3. The elements iron (Fe) and minerals such as goethite, hematite, and talc play significant roles in the enrichment process, alongside intensive weathering. The zones of enrichment, elemental relationships, and mineralogy of scandium are well-defined; however, the specific form of elemental bonding of scandium with goethite, hematite, and talc requires further analysis. In harzburgitic rocks, scandium is primarily hosted in augite, which has the chemical formula $(Ca,Na)(Mg,Fe,Al,Ti)(Si,Al)_2O_6$. Augite crystallizes through exsolution processes driven by variations in the aluminum content of the magma. Elevated aluminum concentrations favor the formation of augite, whereas diopside tends to form during aluminum depletion. Given their similar trivalent ionic states, Sc^{3+} and Al^{3+} can readily substitute for each other in the magmatic or silicate melt phase. This geochemical affinity indicates that augite serves as a primary mineral host for scandium during magmatic differentiation.

Within the nickel laterite profile, scandium is not incorporated through isomorphous substitution with iron or magnesium, but rather adsorbed onto iron oxide phases and, to a lesser extent, onto Al-bearing minerals. In the weathered zone, scandium is also associated with manganese and aluminum phases. Scandium forms relatively immobile complexes with iron oxides, resulting in its accumulation in the upper portion of the laterite profile, particularly within the Fe-rich limonite zone.

References

[1] Perkins D. et al, *Mineralogy*. Grand Forks, ND: University of North Dakota, 2020.

[2] S. Al Khirbash and K. Semhi, "Mobilization and redistribution of elements in laterites of Semail ophiolite, Oman: A mass balance study," *Sultan Qaboos University Journal for Science*, vol. 20, no. 1, pp. 39-54, 2015. https://doi.org/10.24200/squjs.vol20iss1pp39-54

[3] Y. Teitler, M. Cathelineau, M. Ulrich, J. Ambrosi, M. Munoz, and B. Sevin, "Petrology and geochemistry of scandium in New Caledonian Ni-Co laterites," *Journal of Geochemical Exploration*, vol. 196, pp. 131-155, 2019. https://doi.org/10.1016/j.gexplo.2018.10.009

[4] T. Simandjuntak and A. Barber, "Contrasting tectonic styles in the Neogene orogenic belts of Indonesia," *Geological Society, London, Special Publications*, vol. 106, no. 1, pp. 185-201, 1996.

[5] C. Monnier, J. Girardeau, R. C. Maury, and J. Cotten, "Back-arc basin origin for the East Sulawesi ophiolite (eastern Indonesia)," *Geology*, vol. 23, no. 9, pp. 851-854, 1995. https://doi.org/10.1130/0091-7613(1995)023<0851:BABOFT>2.3.CO;2

[6] C. Parkinson, "Emplacement of the East Sulawesi Ophiolite: evidence from subophiolite metamorphic rocks," *Journal of Asian Earth Sciences*, vol. 16, no. 1, pp. 13-28, 1998. https://doi.org/10.1016/S0743-9547(97)00039-1

[7] R. Harris, "Geodynamic patterns of ophiolites and marginal basins in the Indonesian and New Guinea regions," *Geological Society, London, Special Publications*, vol. 218, no. 1, pp. 481-505, 2003.

[8] A. Kadarusman, S. Miyashita, S. Maruyama, C. D. Parkinson, and A. Ishikawa, "Petrology, geochemistry and paleogeographic reconstruction of the East Sulawesi Ophiolite, Indonesia," *Tectonophysics*, vol. 392, no. 1-4, pp. 55-83, 2004. https://doi.org/10.1016/j.tecto.2004.04.008

[9] Surono, "Geology of the Southeastern arm of sulawesi," Bandung, Indonesia: Geological Agency of the Ministry of Energy and Mineral Resources of the Republic of Indonesia, 2013.

[10] U. G. T. D. Tim Eksplorasi Nikel Sulawesi Tenggara, "Final report on nickel laterite exploration in the Tapunopaka and east lalindu areas of southeast sulawesi province of New Caledonia," *Journal of Geochemical Exploration*, 2021.

[11] Y. H. Paskarino, Sutarto, J. Soesilo, B. Sutopo, and O. C. Situmorang, "Potential indication of scandium in the limonite zone at Tapunopaka block, North Konawe, Southeast Sulawesi," *AIP Conference Proceedings*, vol. 3019, no. 1, p. 040004, 2024. https://doi.org/10.1063/5.0224041

[12] A. Streckeisen, "To each plutonic rock its proper name," *Earth-Science Reviews*, vol. 12, no. 1, pp. 1-33, 1976.

[13] Z. Liu *et al.*, "Study of e+ e-⟶ π+ π-J/ψ and Observation of a Charged Charmoniumlike State at Belle," *Physical Review Letters*, vol. 110, no. 25, p. 252002, 2013.

[14] A. Waheed, *Laterites: Fundamental of chemistry, mineralogy, weathering processes, formation and exploration*. Sudbury, ON, Canada: Vale Inco, 2008.

[15] P. Young, "Tables of functions for a spherical galaxy obeying the 7-1/1 law in projection," *Astronomical Journal*, vol. 81, p. 807, 1976.

[16] C. Butt and H. Zeegers, "Climate, geomorphological environment and geochemical dispersion models," *Handbook of Exploration Geochemistry*, vol. 4, pp. 3-24, 1992.

[17] S. R. Pedro and J. M. Camargo, "Meliponini neotropicais: O gênero Partamona schwarz, 1939 hymenoptera, apidae," *Revista Brasileira de Entomologia*, vol. 47, pp. 1-117, 2003.

[18] C. Furtado, *The economic growth of Brazil: A survey from colonial to modern times*. Berkeley, CA: University of California Press, 1968.